INTERNATIONAL JOURNAL FOR NUMERICAL METHODS IN FLUIDS
Int. J. Numer. Meth. Fluids 2008; **56**:661–686
Published online 4 July 2007 in Wiley InterScience (www.interscience.wiley.com). DOI: 10.1002/fld.1546

Analysis of a second-order upwind method for the simulation of solute transport in 2D shallow water flow

J. Murillo[1], P. García-Navarro[1,*,†] and J. Burguete[2]

[1]*Fluid Dynamics, CPS, University of Zaragoza, Spain*
[2]*Agua y Suelo, EEAD, CSIC, Spain*

SUMMARY

A two-dimensional model for the simulation of solute transport by convection and diffusion into shallow water flow over variable bottom is presented. It is based on a finite volume method over triangular unstructured grids. A first-order upwind technique, a second order in space and time and an extended first-order method are applied to solve the non-diffusive terms in both the flow and solute equations and a centred implicit discretization is applied to the diffusion terms. The stability constraints are studied and the form to avoid oscillatory results in the solute concentration in the presence of complex flow situations is detailed. Some comparisons are carried out in order to show the performance in terms of accuracy of the different options. Copyright © 2007 John Wiley & Sons, Ltd.

Received 4 October 2006; Revised 30 April 2007; Accepted 12 May 2007

KEY WORDS: solute transport; convection; diffusion; shallow water flow; source terms; coupled system; finite volumes; two-dimensional model; conservation

1. INTRODUCTION

In the modelling of passive solute transport by shallow water flows, for low concentrations, the solute dynamics does not influence the flow behaviour [1]. It has been previously studied [2] that, despite the widespread tendency to the use of a simple sequential decoupled resolution algorithm, as in the context of semi-Lagrangian methods [3, 4], it is preferable, in the context of Eulerian conservative upwind schemes, to use a coupled formulation for the advective part. Second-order schemes for the coupled system are the next step towards an improved solution specially when there is an interest in the accurate tracking of a localized initial solute distribution transported by the flow. However, it is common in the literature to speak of the convenience of applying

*Correspondence to: P. García-Navarro, Fluid Dynamics, CPS, University of Zaragoza, Spain.
†E-mail: pigar@unizar.es

Contract/grant sponsor: INCLAM company
Contract/grant sponsor: Spanish Ministry of Science and Education; contract/grant number: CGL2005-07059-C02-02

second-order schemes to the complete two-dimensional (2D) set of dynamic equations including source terms, non-linearity, irregular geometries and dry areas when the property of second order of accuracy of those schemes is only ensured for the simple case of a scalar linear homogeneous equation in one dimension. Accuracy, conservation and numerical stability are central properties of a numerical method and must be carefully considered when trying to understand how they interfere with each other.

Oliveira and Fortunato [5] tested 10 numerical schemes in an Eulerian–Lagrangian control volume finite element model over 2D test cases of varying complexity finding that the method of choice depends on the problem being solved and on the grid resolution.

Begnudelli and Sanders [6] modelled shallow water flow and scalar transport over arbitrary topography using a second-order upwind scheme and involving wetting/drying fronts and reported that scalar predictions cannot be accurately predicted as undershoots and overshoots were generated even in cases with initial constant values of scalar concentration, requiring water depth and scalar concentration tolerances to avoid an excessive mass error.

In this work, a continuation of a previous effort on the development of conservative upwind schemes for triangular meshes using first-order methods limited or not by the Courant–Friedrichs–Levy CFL<1 [7] restriction [8] over irregular and dry geometries that do not affect the size of the allowable time step or the quality of the solution [9] and their extension to second order of accuracy [10] is presented. In Murillo *et al.* [9] it was realized that the solute transport advancing fronts in the shallow water body require special numerical treatment in some cases, particularly when the solute concentration discontinuity is located at the same place as a water depth discontinuity. Although the numerical solutions for the conserved variables supplied by the numerical scheme are always monotone, this is not the case for the solute concentration. This is true when using a first-order scheme but also, and even more difficult to cure, when moving to a second-order approach.

The interest of this work is focused on the rigorous comparison of all the options in order to ascertain the true effect of using a second-order representation. For that purpose, steady and unsteady test cases have been selected with smooth and discontinuous solutions.

2. GOVERNING EQUATIONS

The solute transport and water flow under shallow conditions can be formulated by means of the depth-averaged set of equations expressing water volume conservation, solute volume conservation and water momentum conservation. Following Murillo *et al.* [2], the system of partial differential equations will be formulated here in coupled form as follows:

$$\frac{\partial \mathbf{U}}{\partial t} + \frac{\partial \mathbf{F}(\mathbf{U})}{\partial x} + \frac{\partial \mathbf{G}(\mathbf{U})}{\partial y} = \mathbf{T}(\mathbf{U}) \tag{1}$$

being

$$\mathbf{U} = (h, q_x, q_y, h\phi)^{\mathrm{T}}$$
$$\mathbf{F} = \left(q_x, \frac{q_x^2}{h} + \frac{gh^2}{2}, \frac{q_x q_y}{h}, h\phi u\right)^{\mathrm{T}}, \quad \mathbf{G} = \left(q_y, \frac{q_x q_y}{h}, \frac{q_y^2}{h} + \frac{gh^2}{2}, h\phi v\right)^{\mathrm{T}} \tag{2}$$
$$\mathbf{T} = (0, gh(S_{ox} - S_{fx}), gh(S_{oy} - S_{fy}), \vec{\nabla}(\mathbf{K}h\vec{\nabla}\phi))^{\mathrm{T}}$$

DOI: 10.1002/fld

where h is the water depth, g is the acceleration of the gravity, $q_x = uh$, $q_y = vh$ the unit discharge components, with (u, v) the averaged components of the velocity vector $\mathbf{u}$ along the x and y coordinates, respectively, and ϕ is the depth-averaged concentration.

The source terms are the bed slopes of the bottom level z,

$$S_{ox} = -\frac{\partial z}{\partial x}, \quad S_{oy} = -\frac{\partial z}{\partial y} \tag{3}$$

the friction losses, written in terms of the Manning's roughness coefficient n [11–13]

$$S_{fx} = \frac{n^2 u|\mathbf{u}|}{h^{4/3}}, \quad S_{fy} = \frac{n^2 v|\mathbf{u}|}{h^{4/3}} \tag{4}$$

and the solute concentration diffusion, where $\mathbf{K}$ is an empirical dispersion matrix that should not be confused with the turbulent diffusivity. In general, $\mathbf{K}$ incorporates dispersion due to differential advection as well as turbulent diffusion [14].

System (2) is time dependent, non-linear, and contains advection, diffusion and source terms. Under the hypothesis of dominant advection it can be classified and numerically dealt with as belonging to the family of hyperbolic systems, The mathematical properties of (2) include the existence of a Jacobian matrix, $\mathbf{J}_n$, of the projected flux $(\mathbf{En})$ defined as

$$\mathbf{J}_n = \frac{\partial(\mathbf{En})}{\partial \mathbf{U}} = \frac{\partial(\mathbf{F})}{\partial \mathbf{U}} n_x + \frac{\partial(\mathbf{G})}{\partial \mathbf{U}} n_y \tag{5}$$

where $\mathbf{n}$ is a unit vector indicating a certain direction. This Jacobian can be used to form the basis of the finite volume upwind numerical discretization that will be outlined in the next section. There $\mathbf{n}$ will be the unit normal to the cell side and $(\mathbf{En})$ the normal flux.

3. NUMERICAL MODEL

The existence of the Jacobian matrix and the differential relation among conserved variables, fluxes and Jacobian allows a local linearization of the form

$$\delta(\mathbf{En})_k = \widetilde{\mathbf{J}}_n \delta \mathbf{U}_k \tag{6}$$

that will be applied in the context of a finite volume formulation at every cell edge k separating cell i and j. As suggested by Roe [15] the matrix $\widetilde{\mathbf{J}}_n$ has the same shape as $\mathbf{J}_n$ but is evaluated at an average state defined by the edge average quantities $\widetilde{\mathbf{u}} = (\widetilde{u}, \widetilde{v})$, $\widetilde{c}$ and $\widetilde{\phi}$, which must be calculated according to the set of the matrix properties [2]. The eigenvalues of $\widetilde{\mathbf{J}}_n(\mathbf{U}_i, \mathbf{U}_j)$ are

$$\widetilde{\lambda}^1 = \widetilde{\mathbf{u}}\mathbf{n} + \widetilde{c}, \quad \widetilde{\lambda}^2 = \widetilde{\mathbf{u}}\mathbf{n}, \quad \widetilde{\lambda}^3 = \widetilde{\mathbf{u}}\mathbf{n} - \widetilde{c}, \quad \widetilde{\lambda}^4 = \widetilde{\mathbf{u}}\mathbf{n} \tag{7}$$

and the corresponding eigenvectors

$$\widetilde{\mathbf{e}}^1 = \begin{pmatrix} 1 \\ \widetilde{u} + \widetilde{c}n_x \\ \widetilde{v} + \widetilde{c}n_y \\ \widetilde{\phi} \end{pmatrix}, \quad \widetilde{\mathbf{e}}^2 = \begin{pmatrix} 0 \\ -\widetilde{c}n_y \\ \widetilde{c}n_x \\ 0 \end{pmatrix}, \quad \widetilde{\mathbf{e}}^3 = \begin{pmatrix} 1 \\ \widetilde{u} - \widetilde{c}n_x \\ \widetilde{v} - \widetilde{c}n_y \\ \widetilde{\phi} \end{pmatrix}, \quad \widetilde{\mathbf{e}}^4 = \begin{pmatrix} 0 \\ 0 \\ 0 \\ 1 \end{pmatrix} \tag{8}$$

DOI: 10.1002/fld

The difference in vector $\mathbf{U}$ across the grid edge is projected onto the matrix eigenvectors basis so that, the difference at the edge k of cell i is $\delta\mathbf{U}_{i,k} = \sum_{m=1}^{4} (\alpha\tilde{\mathbf{e}})_{i,k}^{m}$, so that the coefficients α^m are

$$\alpha^{1,3} = \frac{\delta h}{2} \pm \frac{1}{2\tilde{c}}(\delta\mathbf{q} - \tilde{\mathbf{u}}\delta h)\mathbf{n}, \quad \alpha^2 = \frac{1}{\tilde{c}}(\delta\mathbf{q} - \tilde{\mathbf{u}}\delta h)\mathbf{n}_{\mathrm{t}}, \quad \alpha^4 = \delta(h\phi) - \tilde{\phi}(\delta h) \tag{9}$$

where $\mathbf{q} = (q_x, q_y)$, $\mathbf{n}$ is the unit normal vector pointing outward to cell i and $\mathbf{n}_{\mathrm{t}}$ is the unit tangential vector to the edge, $\mathbf{n}_{\mathrm{t}} = (-n_y, n_x)$ and all the spatial increments represent differences between the neighbour cells and cell i, $\delta f_{i,k} = f_j - f_i$.

For this reason, (6) becomes $\delta(\mathbf{En})_k = \sum_{m=1}^{4} (\tilde{\lambda}\alpha\tilde{\mathbf{e}})_{i,k}^{m}$.

The diagonalization matrices of $\tilde{\mathbf{J}}_n = \tilde{\mathbf{P}}\tilde{\mathbf{\Lambda}}\tilde{\mathbf{P}}^{-1}$, where $\tilde{\mathbf{\Lambda}}$ is a diagonal matrix consisting of the eigenvalues given in (7), are:

$$\tilde{\mathbf{P}} = \begin{pmatrix} 1 & 0 & 1 & 0 \\ \tilde{u} + \tilde{c}n_x & -\tilde{c}n_y & \tilde{u} - \tilde{c}n_x & 0 \\ \tilde{v} + \tilde{c}n_y & \tilde{c}n_x & \tilde{v} - \tilde{c}n_y & 0 \\ \tilde{\phi} & 0 & \tilde{\phi} & 1 \end{pmatrix}, \quad \tilde{\mathbf{P}}^{-1} = \frac{1}{2\tilde{c}} \begin{pmatrix} -\tilde{\mathbf{u}}\mathbf{n} + c & n_x & n_y & 0 \\ 2(\tilde{u}n_y - \tilde{v}n_x) & -2n_y & 2n_x & 0 \\ \tilde{\mathbf{u}}\mathbf{n} + c & -n_x & -n_y & 0 \\ -2\tilde{\phi}\tilde{c} & 0 & 0 & 2\tilde{c} \end{pmatrix} \tag{10}$$

They can be used to upwind the rest of the terms in the equation, considering them all as source terms. The bed and friction source terms are expressed as $-\vec{\nabla}z$ and $\vec{\nabla}H$, respectively, while the diffusion source term is written as $\mathbf{Dif} = \mathbf{K}h\vec{\nabla}\phi$ or $\mathbf{Dif} = (\mathrm{Dif}_x, \mathrm{Dif}_y)$. The normal source difference is

$$\delta\mathbf{Tn} = \delta(\mathbf{S}_1, \mathbf{S}_2)^{\mathrm{T}}\mathbf{n} = \begin{pmatrix} 0 \\ g\tilde{h}(-\delta z + \delta H)n_x \\ g\tilde{h}(-\delta z + \delta H)n_y \\ \delta\mathbf{Dif}\,\mathbf{n} \end{pmatrix} \tag{11}$$

where the auxiliary matrices $\mathbf{S}_1$ and $\mathbf{S}_2$ are evaluated at every interior edge as

$$\mathbf{S}_1 = (0, g\tilde{h}(-z + H), 0, \mathrm{Dif}_x)^{\mathrm{T}}, \quad \mathbf{S}_2 = (0, 0, g\tilde{h}(-z + H), \mathrm{Dif}_y)^{\mathrm{T}} \tag{12}$$

and where $\tilde{h} = \frac{1}{2}(h_i + h_j)$.

All of the source terms can also be projected onto the basis of eigenvectors using the following coefficients:

$$\boldsymbol{\beta} = \tilde{\mathbf{P}}^{-1}(\delta\mathbf{Tn}) = \frac{1}{2\tilde{c}} \begin{pmatrix} g\tilde{h}(-\delta z + \delta H) \\ 0 \\ -g\tilde{h}(-\delta z + \delta H) \\ \delta\mathbf{Dif}\,\mathbf{n} \end{pmatrix} \tag{13}$$

so that the coefficients β^m are defined as

$$\beta^1 = -\frac{\tilde{c}}{2}(\delta z + d_n S_f), \quad \beta^1 = -\beta^3, \quad \beta^2 = 0, \quad \beta^4 = \delta\,\mathbf{Dif}\,\mathbf{n} \tag{14}$$

where d_n is distance between cell centres projected on $\mathbf{n}$ [9].

DOI: 10.1002/fld

3.1. First-order approach

The tools presented in the preceding section can be combined to produce the fully upwind first-order scheme in a form that was already reported for the one-dimensional (1D) shallow water equations, for instance, in [16] and for the 1D and 2D shallow water equations in [17]. The same form was adopted for the coupled 2D shallow water/solute transport system and reported in [2]. It is formulated as follows:

$$\mathbf{U}_i^{n+1} = \mathbf{U}_i^n - \sum_{k=1}^{\mathrm{NE}} \sum_{m=1}^{4} ((\widetilde{\lambda}^{m-} \alpha^m - \beta^{m-}) \widetilde{\mathbf{e}}^m)_i^n \frac{l_k}{A_i} \Delta t \tag{15}$$

where l_k is the k edge length and A_i the area of cell i. This scheme is based on condition (6) where the negative part of

$$\widetilde{\lambda}^{\pm m} = \tfrac{1}{2}(\widetilde{\lambda}^m \pm |\widetilde{\lambda}^m|) \tag{16}$$

and that of

$$\delta \mathbf{T}\mathbf{n}_k^{\pm} = \widetilde{\mathbf{P}}(\mathbf{I} \pm |\widetilde{\mathbf{\Lambda}}|\widetilde{\mathbf{\Lambda}}^{-}) \widetilde{\mathbf{P}}^{-1} \delta \mathbf{T}\mathbf{n} = \sum_{m=1}^{4} \beta^{m\pm} \widetilde{\mathbf{e}}^m \tag{17}$$

are the only one used to update every cell [2].

The expression in (15) corresponds to a fully upwind first-order scheme but is not appropriate for the discretization of the diffusive term. The discretization indicated by (11) and (13) means that diffusion is controlled by the eigenvalue associated with $\widetilde{\mathbf{e}}^4$, $\widetilde{\lambda}_4 = \widetilde{\mathbf{u}}\,\mathbf{n}$ or, otherwise, that diffusion is neglected in any direction different from the normal advection velocity. This leads to incorrect results. We propose that the diffusion term is extracted from the upwind scheme and, within the context of a finite volume method, first transformed into a contour integral over the cell edges

$$\int_{\Omega_i} \vec{\nabla}(\mathbf{K} h \vec{\nabla}\phi) \partial\Omega = \int_{\partial\Omega_i} (\mathbf{K} h \vec{\nabla}\phi)\, \mathbf{n}\, \mathrm{d}l \tag{18}$$

so that it can be approximated as

$$\sum_{k=1}^{\mathrm{NE}} \left(\mathbf{K} \widetilde{h} \frac{\delta\phi}{d_n} \mathbf{n} \right)_k \mathbf{n}_k l_k \tag{19}$$

which is a second-order approach on a quadrilateral structured grid, and has been adapted to the triangular geometry. Using a splitting technique, in a first step, scheme (15) can be applied to the non-diffusive system, that is, using:

$$\boldsymbol{\beta} = \widetilde{\mathbf{P}}^{-1}(\delta \mathbf{T}\mathbf{n}) = \frac{1}{2\widetilde{c}} \begin{pmatrix} g\widetilde{h}\,(-\delta z + \delta H) \\ 0 \\ -g\widetilde{h}\,(-\delta z + \delta H) \\ 0 \end{pmatrix} \tag{20}$$

After solving the non-diffusive system in a first step and obtaining a predicted value of the conserved variables, that will be denoted ϕ^* for the solute concentration, the final value of ϕ^{n+1} including diffusion is computed by means of an implicit method over the diffusion term in a second step.

DOI: 10.1002/fld

The numerical diffusion step becomes unconditionally stable, as the resolution matrix is positive definite, so finally the time step used depends only on the value of CFL as if only advection was involved. Then,

$$\frac{(h\phi)_i^{n+1} - (h\phi)_i^*}{\Delta t} A_i = \sum_{k=1}^{\mathrm{NE}} \left(\mathbf{K} \widetilde{h} \frac{\delta\phi}{d_n} \mathbf{n} \right)_k^{n+1} \mathbf{n}_k l_k \tag{21}$$

where $h_i^{n+1} = h_i^*$. (21) in cases of $h_i^{n+1} \neq 0$ can be rewritten as

$$\phi_i^{n+1} = \phi_i^* + \sum_{k=1}^{\mathrm{NE}} \left((\mathbf{Kn})\mathbf{n} \frac{\widetilde{h} l_k}{h_i d_n A_i} \Delta t \right)_k^{n+1} \delta\phi_k^{n+1} = \phi_i^* + \sum_{k=1}^{\mathrm{NE}} C_{i,k}^{n+1} \delta\phi_k^{n+1} \tag{22}$$

where each coefficient $C_{i,k}^{n+1}$ is known. Finally:

$$\phi_i^{n+1} = \frac{\phi_i^* + \sum_{k=1}^{\mathrm{NE}} C_{i,k}^{n+1} \phi_k^{n+1}}{1 + \sum_{k=1}^{\mathrm{NE}} C_{i,k}^{n+1}} \tag{23}$$

As each $C_{i,k}^{n+1} \geqslant 0$ the system of equations is unconditionally stable. It can be easily solved using an iterative scheme [2], assuming that in the initial step $\phi_i^{n+1} = \phi_i^*$.

3.2. Second-order approach

A second-order upwind approach for the non-diffusive system can be based on the so-called MUSCL–Hancock scheme [18] formulated as based on the first-order scheme presented in the previous section but achieving better accuracy by means of two steps. In the first step, the solution must be linearly reconstructed by cells using the $\mathbf{L}_i$ gradient vectors

$$\mathbf{U}_i(x, y) = \mathbf{U}_i(x_0, y_0) + \mathbf{r}(x, y)\mathbf{L}_i = \mathbf{U}_{i,0} + \mathbf{r}(x, y)\mathbf{L}_i \tag{24}$$

The slope of these gradient functions is limited according to the maximum limited gradient (MLG) and MLG–Wierse limiting functions [19, 20] then intermediate values $\mathbf{U}_{I,k}^{n+1/2}$ are re-calculated at a half time step at cell edges as

$$\mathbf{U}_{I,k}^{n+1/2} = \mathbf{U}_{I,k}^n - \sum_{k=1}^{\mathrm{NE}} (\delta\mathbf{E}\mathbf{n}_k - \delta\mathbf{T}\mathbf{n}_k)_{Ii,k}^n \frac{l_k}{A_i} \frac{\Delta t}{2} \tag{25}$$

which is equivalent to redefining the interpolation function in each cell. Figure 1 illustrates the cell-wise linear reconstructions and clarifies the meaning of the notation. For more details see [10]. The updated variable is constructed in a second step as

$$\mathbf{U}_i^{n+1} = \mathbf{U}_i^n - \sum_{k=1}^{\mathrm{NE}} (\delta\mathbf{E}\mathbf{n}_k - \delta\mathbf{T}\mathbf{n}_k)_{JI,k}^{n+1/2,-} \frac{l_k}{A_i} \Delta t - \sum_{k=1}^{\mathrm{NE}} (\delta\mathbf{E}\mathbf{n}_k - \delta\mathbf{T}\,\mathbf{n}_k)_{Ii,k}^{n+1/2} \frac{l_k}{A_i} \Delta t \tag{26}$$

where $\delta\mathbf{E}_{JI,k}^{n+1/2} = \mathbf{E}_{J,k}^{n+1/2} - \mathbf{E}_{I,k}^{n+1/2}$ and $\delta\mathbf{E}_{Ii,k}^{n+1/2} = \mathbf{E}_{I,k}^{n+1/2} - \mathbf{E}_{i,k}^n$, with an upwind part (first term) and a central part (second term). The above described (21)–(23) implicit procedure for the diffusion term discretization must be then used as stated.

DOI: 10.1002/fld

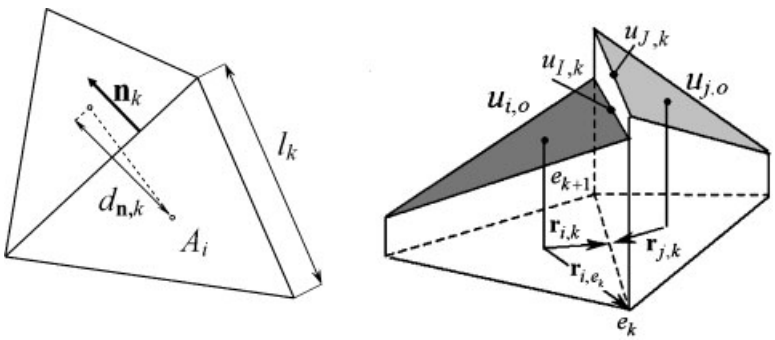

Figure 1. Cell geometry parameters (left) and linear representation by cells (right).

3.3. Numerical stability

When analysing both first- and second-order approaches for the non-diffusive system in Sections 3.1 and 3.2 the conditions to preserve the sign and the monotonicity of the variables in the presence of source terms and dry/wet fronts are relevant. For the shallow water equations alone, these were studied in detail in [10]. Now these conditions must be extended to the new conserved variable, the solute mass ($h\phi$), and, nonetheless, our interest is also to enforce the good properties to the primitive variable ϕ, guaranteeing that

$$\phi_k^{\min} \leqslant \phi_i^{n+1} \leqslant \phi_k^{\max} \tag{27}$$

where $\phi_k^{\max} = \max\{\phi_{i,0}, \phi_{j,0}\}_k$ and $\phi_k^{\min} = \min\{\phi_{i,0}, \phi_{j,0}\}_k$ in all situations and under both first-order and second-order accuracy. The properties of the coupled Jacobian matrix guarantee (27) in the presence of an initial constant solute concentration, but this property does not hold in general.

In [10], the second-order approach (25) was rewritten as follows:

$$\mathbf{U}_i^{n+1} = \mathbf{U}_i^n - \sum_{k=1}^{\mathrm{NE}} \sum_{m=1}^{N\lambda} (v^* \delta \mathbf{U})_{JI,k}^m - \sum_{k=1}^{\mathrm{NE}} \sum_{m=1}^{N\lambda} (v^* \delta \mathbf{U})_{Ii,k}^m \tag{28}$$

where $N\lambda$ is the number of eigenvalues, $N\lambda = 4$ in our case, and

$$v_{JI,k}^m = \frac{\lambda_{JI,k}^{m,*}}{(A_i / l_k)} \Delta t, \quad v_{Ii,k}^m = \frac{\lambda_{Ii,k}^{m,*}}{(A_i / l_k)} \Delta t \tag{29}$$

with

$$\tilde{\lambda}_{JI,k}^* = \tilde{\lambda}_{JI,k}^- \theta_{JI,k}, \quad \theta_{JI,k} = 1 - \left(\frac{\beta}{\alpha \tilde{\lambda}} \right)_{JI,k}^-, \quad \tilde{\lambda}_{Ii,k}^* = \tilde{\lambda}_{Ii,k}^- \theta_{Ii,k}, \theta_{Ii,k} = 1 - \left(\frac{\beta}{\alpha \tilde{\lambda}} \right)_{Ii,k}^- \tag{30}$$

in order to study the influence of the source terms in the stability condition. It was stated that the stability condition for the explicit time integration was

$$\begin{gathered} \Delta t = \mathrm{CFL}\, \Delta t_{\max}, \quad \mathrm{CFL} \leqslant \tfrac{1}{3} \\ \Delta t_{\max} = \min\{\Delta t_k\}_{k=1,N\mathrm{edge}}, \quad \Delta t_k = \frac{A_{\min,k}}{\max_m \{\lambda_{k,\max}^{m,*}\} l_k}, \quad m = 1, \ldots, 4 \end{gathered} \tag{31}$$

DOI: 10.1002/fld

with $A_{\min,k} = \min\{A_i, A_j\}$, the minimum area of the two cells sharing edge k, and $\lambda^{m,*}_{k,\max} = \max\{|\lambda^*_{JI,k}|, |\lambda^*_{Ii,k}|, |\lambda^*_k|\}$, considering that the coefficients θ^m_k are positive. When $\theta^m_k < 0$ the source terms dominate over the flux differences and a coefficient γ based on the specific necessity of preserving the sign over the solution in the s component, expressed as

$$\begin{aligned} U^{n+1}_{s,i} \leqslant 0, \quad U^n_{s,i}, U^n_{s,j=1,2,3} \leqslant 0 \\ U^{n+1}_{s,i} \geqslant 0, \quad U^n_{s,i}, U^n_{s,j=1,2,3} \geqslant 0 \end{aligned} \tag{32}$$

was introduced so that

$$\Delta t_k = \gamma \frac{A_{\min,k}}{\max_m\{|\lambda^{m,*}_k|\} l_k}, \quad \gamma = \frac{\min_{i,j}\{|U_{s,i}|, |U_{s,j}|, |\delta U_s|\}}{|\delta U_s|} \tag{33}$$

When moving to the coupled set of water flow and solute transport equations, γ is defined with the same purpose in this case as:

$$\begin{gathered} \gamma = \min\{\gamma_h, \gamma_{h\phi}\} \\ \gamma_h = \frac{\min\{h_{i,0}, h_{j,0}, |\delta h_k|\}}{|\delta h_k|}, \quad \gamma_{h\phi} = \frac{\min\{(h\phi)_{i,0}, (h\phi)_{j,0}, |\delta(h\phi)_k|\}}{|\delta(h\phi)_k|} \end{gathered} \tag{34}$$

In Murillo *et al.* [10], when analysing second-order approach observing the conservation and positivity of the water depth, the numerical scheme was reduced to first order in those cases where $0 \leqslant \gamma < 1$ and $\theta^m_k < 0$. When the system of equations is extended to include solute transport the same conclusions are met. On the other hand, the reduction of the time step when $0 < \gamma < 1$ can be avoided using a conservative redistribution of the updating contributions for both water depth and solute mass [9]. In the particular case $\gamma = 0$ the theory predicts that no flux of information can cross the edge, acting as a solid wall in wetting/drying fronts. In the presence of solute fronts, that is, clean/mixed water boundaries with continuous water level surface this leads to unrealistic results in the solute advance. If this fact is not considered, negative values of solute mass and concentration can be obtained and the necessity to tune and alter the scheme's results becomes necessary. This can be avoided using again a conservative redistribution of the updating contributions [9] that ensures adequate bounding properties over the solute concentration.

In Murillo *et al.* [10] interpolation over the water level surface was required in the presence of variable bed level, and in some special cases the numerical scheme was reduced to first-order approach. In those cases it is also necessary to enforce first order over the solute mass too.

The value of ϕ is computed as the ratio between the variables $h\phi$ and h, for both first- and second-order approximations. If second order is imposed over h and $h\phi$ the final value of the solute concentration ϕ depends on the interpolation functions used and unrealistic values of solute concentration can appear. The oscillations in the solute concentration can be avoided by reducing the scheme to first order when the solute concentration defined at the edges does not fulfil the following condition:

$$\phi_{\min} \leqslant \phi_{I,k} \leqslant \phi_{\max} \tag{35}$$

where $\phi_{\min} = \min\{\phi_{i,0}, \phi_{j,0}\}$ and $\phi_{\max} = \max\{\phi_{i,0}, \phi_{j,0}\}$. In the presence of strong spatial variations in the water depth this technique is overly restrictive and leads to a first-order solution. When this option is not desirable, extrapolation of the solute concentration ϕ keeping first order over the

DOI: 10.1002/fld

water depth is another possibility. This option provides the most accurate results regarding solute concentration. As our interest is focused on keeping the maximum accuracy over the transported solute function the interpolation must be constructed preserving (35).

It must be signalled that the average solute concentration $\widetilde{\phi}$ is independent of the eigenvalues of the system and has no influence on the fluid dynamics. On the other hand, the flow dynamics determines the solute concentration map. A solution that provides second order for both the flow movement and the solute transport is not feasible, and the user has to choose in each case between the cited strategies.

3.4. Extension of the first order scheme to values of CFL>1

Solute transport processes are usually simulated involving large time scales, and, therefore, it is important to enlarge the stability region as much as possible. In the context of fixed boundaries and unstructured triangular meshes, the classical first-order explicit upwind finite volume scheme is forced to follow the criterion CFL$\leqslant$1.

In [8], the stability region of the first-order upwind finite volume scheme for systems of conservation laws was extended to values of CFL greater than one. The basic procedure relies on the enlargement of the stencil for each different contribution $\delta \mathbf{U}_{i,k}^m$. When the method is applied to the shallow water equations, the scheme proves accurate and reduces efficiently the computational cost. In the case of the coupled shallow water/solute transport equations the definition of the new Jacobian matrix makes feasible the use of this new upwinding technique.

According to [8] the updating formula in (15) takes the form

$$\mathbf{U}_i^{n+1} = \mathbf{U}_i^n - \sum_{k=1}^{\mathrm{NE}} \sum_{m=1}^{4} (\nu^m \delta \mathbf{U}^m + \boldsymbol{\kappa}^m \Delta t)_k^n \tag{36}$$

where

$$\nu^m = \lambda^{m-}(l_k/A_i)\Delta t, \quad \boldsymbol{\kappa}^m = \beta^m \widetilde{\mathbf{e}}^m (l_k/A_i) \tag{37}$$

are defined for the m eigenvalues. Depending on the size of the time step used, a new stencil for each component of $\delta \mathbf{U}_k$, $\delta \mathbf{U}_k^m$, is defined, where the number of involved cells is

$$N_k^m = \sum_{n=0}^{-\mu_k^m} 2^n \tag{38}$$

with $\mu_k^m = \mathrm{int}(\nu_k^m)$. As the search of the global time step $\Delta t_{\max}$ involves all the eigenvalues, for each value of CFL desired the size of the actual global time step must be computed considering:

$$A_{\min,k}^m = \min\{A_i, A_{j=1,N_k^m-1}\} \tag{39}$$

For more details, see Murillo *et al.* [8].

To avoid unrealistic values in the numerical solution of the concentration, a strategy based on the conservative redistribution of the solute mass fluxes as presented in [9] must be taken into account. The situations where the concentration is unbounded are well identified by the following condition at a cell edge:

$$\widetilde{\lambda}_{i,k}^{-2} = \widetilde{\lambda}_{i,k}^{-4} = (\widetilde{\mathbf{u}}\mathbf{n})_{i,k}^- = 0, \quad (\widetilde{\lambda}\alpha - \beta)_{i,k}^{-3} > 0, \quad \delta\phi_{i,j}^n \neq 0 \tag{40}$$

DOI: 10.1002/fld

so that

$$\begin{gathered}\widetilde{\lambda}^1_{i,k}=(\widetilde{\mathbf{un}}+\widetilde{c})_{i,k}>0, \quad \widetilde{\lambda}^3_{i,k}=(\widetilde{\mathbf{un}}-\widetilde{c})_{i,k}<0\\ \widetilde{\lambda}^{-1}_{i,k}=0, \quad \widetilde{\lambda}^{-2}_{i,k}=0, \quad \widetilde{\lambda}^{-3}_{i,k}<0, \quad \widetilde{\lambda}^{-4}_{i,k}=0\\ \widetilde{\lambda}^1_{j,k}=-\widetilde{\lambda}^3_{i,k}>0, \quad \widetilde{\lambda}^3_{j,k}=-\widetilde{\lambda}^1_{i,k}<0\\ \widetilde{\lambda}^{-1}_{j,k}=0, \quad \widetilde{\lambda}^{-2}_{j,k}<0, \quad \widetilde{\lambda}^{-3}_{j,k}<0, \quad \widetilde{\lambda}^{-4}_{j,k}<0\end{gathered} \tag{41}$$

In (36), the numerical stencil is enlarged separately for each component $\delta\mathbf{U}^m_k$. This fact introduces an additional difficulty when trying to adapt the strategy used in Murillo *et al.* [9] to redistribute information between cells i and j avoiding at the same time oscillations in the concentration and preserving conservation. For that reason, a coupled modification of the third approximated eigenvector is proposed. It is redefined differently depending on the updating cells i and j, so that the full set of eigenvectors at edge k is

$$\begin{gathered}\widetilde{\mathbf{e}}^1_{i,k}=\begin{pmatrix}1\\ \widetilde{u}+\widetilde{c}n_x\\ \widetilde{v}+\widetilde{c}n_y\\ \widetilde{\phi}\end{pmatrix}_{i,k}, \quad \widetilde{\mathbf{e}}^2_{i,k}=\begin{pmatrix}0\\ -\widetilde{c}n_y\\ \widetilde{c}n_x\\ 0\end{pmatrix}_{i,k}, \quad \widetilde{\mathbf{e}}^3_{i,k}=\begin{pmatrix}1\\ \widetilde{u}-\widetilde{c}n_x\\ \widetilde{v}-\widetilde{c}n_y\\ \widetilde{\phi}_V\end{pmatrix}_{i,k}, \quad \widetilde{\mathbf{e}}^4_{i,k}=\begin{pmatrix}0\\ 0\\ 0\\ 1\end{pmatrix}_{i,k}\\ \widetilde{\mathbf{e}}^1_{j,k}=\begin{pmatrix}1\\ \widetilde{u}+\widetilde{c}n_x\\ \widetilde{v}+\widetilde{c}n_y\\ \widetilde{\phi}\end{pmatrix}_{j,k}, \quad \widetilde{\mathbf{e}}^2_{j,k}=\begin{pmatrix}0\\ -\widetilde{c}n_y\\ \widetilde{c}n_x\\ 0\end{pmatrix}_{j,k}, \quad \widetilde{\mathbf{e}}^3_{j,k}=\begin{pmatrix}1\\ \widetilde{u}-\widetilde{c}n_x\\ \widetilde{v}-\widetilde{c}n_y\\ \widetilde{\phi}_{VV}\end{pmatrix}_{j,k}, \quad \widetilde{\mathbf{e}}^4_{j,k}=\begin{pmatrix}0\\ 0\\ 0\\ 1\end{pmatrix}_{j,k}\end{gathered} \tag{42}$$

where to preserve conservation

$$\widetilde{\phi}_{VV}=\widetilde{\phi}_{j,k}+(\widetilde{\phi}_{i,k}-\phi_V)\frac{(\widetilde{\lambda}\alpha-\beta)^3_{i,k}}{(\widetilde{\lambda}\alpha-\beta)^3_{j,k}} \tag{43}$$

and

$$\phi_V=\begin{cases}\max\{\phi_i,\phi_j\} & \text{if } \delta\phi^n_{i,j}<0 \text{ and } (\widetilde{\lambda}\alpha-\beta)^{-3}_{i,k}>0\\ \min\{\phi_i,\phi_j\} & \text{if } \delta\phi^n_{i,j}>0 \text{ and } (\widetilde{\lambda}\alpha-\beta)^{-3}_{i,k}>0\\ \widetilde{\phi}_{i,k} & \text{else}\end{cases} \tag{44}$$

DOI: 10.1002/fld

This technique will provide accurate and conservative results as will be shown in the Applications section.

4. APPLICATIONS

4.1. Transient solute transport by a uniform discharge over variable bed elevation

The first test case is concerned with the pure advection of an initial solute distribution by means of the velocity field corresponding to a non-uniform steady flow characterized by zero roughness and bi-linear water depth variation. The exact water depth and bottom level distributions corresponding to that situation are:

$$h(x, y) = a + q_x x + q_y y, \quad z(x, y) = -\frac{1}{2g}\frac{(q_x^2 + q_y^2) + 2gh^3}{h^2} \tag{45}$$

The example presented assumes a diagonal discharge with values $q_x = 0.1$, $q_y = 0.1$ and $a = 0.5$ over a squared domain $10 \times 10\,\mathrm{m}^2$, and has been computed using two unstructured meshes, divided into 2064 and 5702 triangular cells. The boundary conditions are, at the upstream sides (south and west in the squared domain), the unit discharges and, at the downstream sides (north and east), the water depth. No diffusion is included and the initial solute concentration distribution is:

$$\phi(x, y, t_0) = \sin\left(\frac{\pi x}{10}\right)\sin\left(\frac{\pi y}{10}\right) \tag{46}$$

The solution for the solute distribution at later times is obtained from the solute transport equation written as

$$h\frac{\partial \phi}{\partial t} + (h\mathbf{u})\vec{\nabla}\phi + \phi\frac{\partial h}{\partial t} + \phi\vec{\nabla}(h\mathbf{u}) = 0 \tag{47}$$

that, using the water mass conservation becomes

$$\frac{\partial \phi}{\partial t} + \mathbf{u}\vec{\nabla}\phi = 0, \quad \frac{\mathrm{d}\phi}{\mathrm{d}t} = 0 \tag{48}$$

which means that the solute concentration is constant along the characteristic curves

$$\frac{\mathrm{d}x}{\mathrm{d}t} = u = \frac{q_x}{h}, \quad \frac{\mathrm{d}y}{\mathrm{d}t} = v = \frac{q_y}{h} \tag{49}$$

As the flow trajectories are known, the advected concentration at a future time $t_0 + T$ can be computed

$$\phi(x', y', t + \Delta t) = \phi(x, y, t) \tag{50}$$

where

$$x'(t + T) = x(t) + \int_t^{t+T} u\,\mathrm{d}t, \quad y'(t + T) = y(t) + \int_t^{t+T} v\,\mathrm{d}t \tag{51}$$

DOI: 10.1002/fld

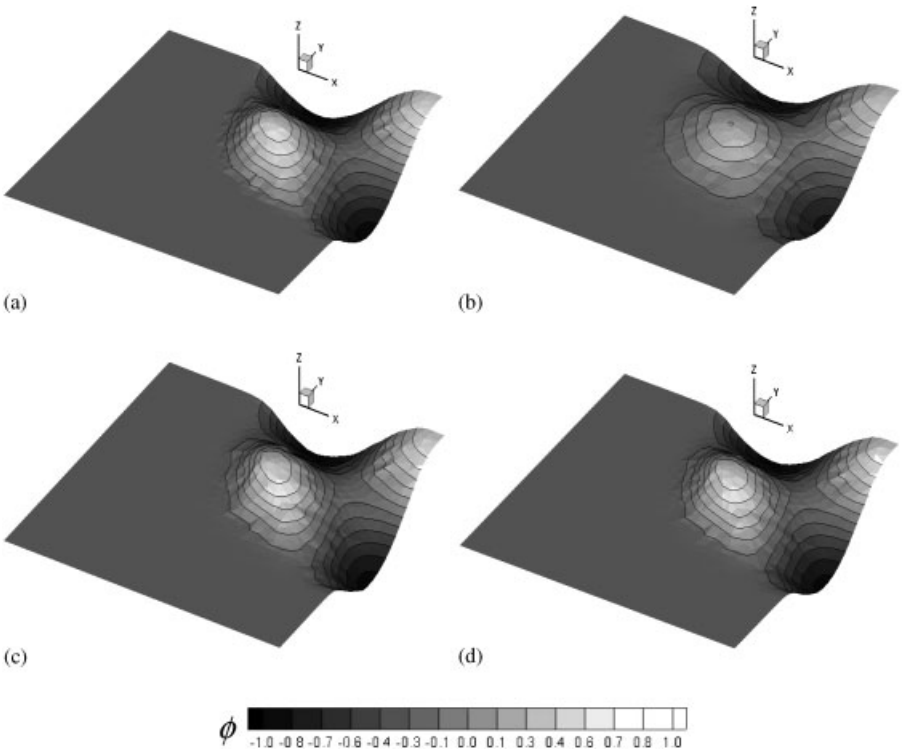

Figure 2. (a) Exact solute concentration; (b) first order with CFL = 2; (c) second order using MLG; and (d) second order using MLG–Wierse.

The particular form of the bed level and water depth functions (45) in this test case correspond to a nearly horizontal water surface level. In consequence, it is almost indifferent to calculate the second-order solution by interpolating the solute concentration or by interpolating the conserved variable. Figure 2(a) shows the solute concentration analytical solution at $t = 50$ s in three-dimensional (3D) view for the mesh with 2064 cells. Figure 2(b) shows the numerical solution obtained using first order with CFL = 2, and Figure 2(c) and (d) the numerical solutions using the second order over the solute concentration and limiters MLG and MLG–Wierse, respectively, with CFL = $\frac{1}{3}$. Visual comparison shows the better quality of the almost identical second-order solutions in this case. Table I shows a quantitative comparison based on the $L_1(\phi)$ error [21] for the different techniques in the two different meshes showing that second order leads distinctly to less diffusive solutions in this test case. When first order is used with different values of CFL, no meaningful differences are found. The non-linear character of the system of equations used produces a rigid uniformity in the results independently of the CFL used.

4.2. Transient solute transport by a non-uniform discharge over variable bed elevation

The second test case is devoted again to the pure advection of an initial solute distribution by a frictionless steady flow over variable bed. In this case, it is characterized by a uniform horizontal

DOI: 10.1002/fld

Table I. $L_1(\phi)$ error for the solute concentration using first and second order.

Cells/L_1	First order (CFL = 1)	First order (CFL = 2)	Second order MLG (CFL = $\frac{1}{3}$)	Second MLG–Wierse (CFL = $\frac{1}{3}$)
2064	4.463	4.469	1.045	0.909
5702	3.066	3.066	0.676	0.592

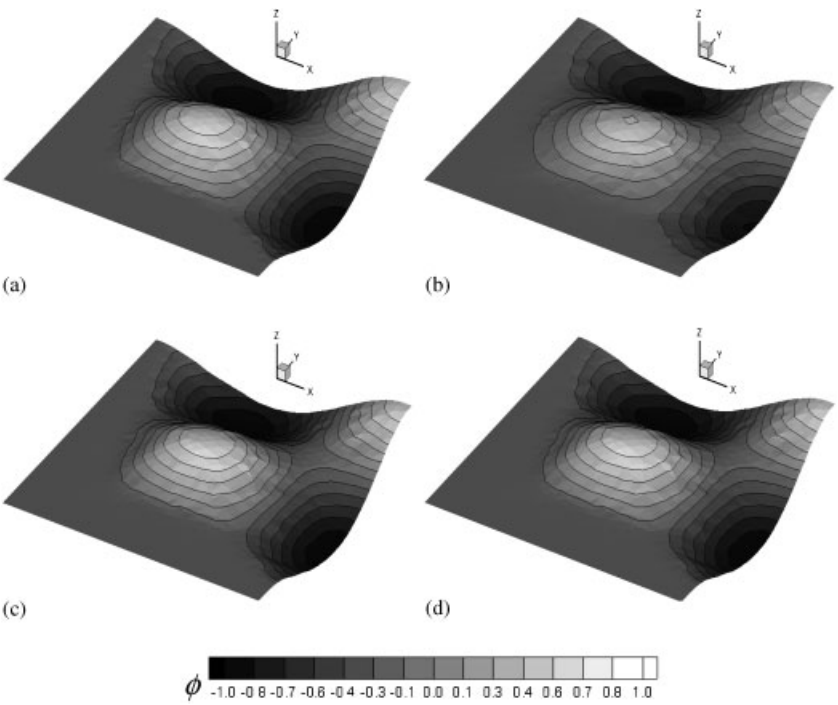

Figure 3. (a) Exact solute concentration; (b) first order with CFL = 2; (c) second order using MLG; and (d) MLG–Wierse.

surface level $\xi(x, y, t) = h + z = 0$. The corresponding bed analytical function is

$$z(x, y) = -h_0 + \frac{q_0}{a} \sin(a\,(x - y)) \tag{52}$$

with unit discharges varying in space as follows:

$$q_x(x, y) = q_y(x, y) = q_0 \cos(a\,(x - y)) \tag{53}$$

The schemes are tested using the values $a = 2\pi/(\sqrt{2}\,30)$, $q_0 = 0.05$ and $h_0 = 3\,q_0/a$. The initial solute distribution, the squared domain size and the meshes are the same as those used in the first test case. The nil gradient water level surface of this case implies that no meaningful differences appear between the solute concentration obtained in second order by interpolating the solute concentration itself or the set of conserved variables. Figure 3(a) shows a 3D view of the analytical

DOI: 10.1002/fld

Table II. $L_1(\phi)$ error for the solute concentration using first and second order.

Cells/L_1	First order (CFL = 1)	First order (CFL = 2)	MLG (CFL = $\frac{1}{3}$)	MLG–Wierse (CFL = $\frac{1}{3}$)
2064	4.413	4.412	1.452	1.297
5702	2.859	2.859	0.928	0.855

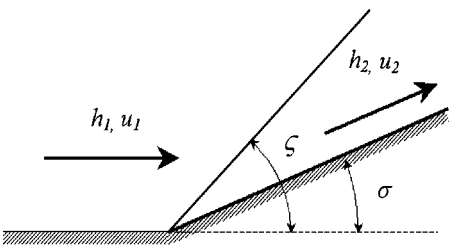

Figure 4. Oblique hydraulic jump.

solution at $t = 50$ s in the mesh with 2064 cells. Figure 3(b) displays the numerical results of solute concentration at that time using first order with CFL = 2. Figure 3(c) and (d) displays the numerical results of solute concentration at that time using second order over the solute concentration with limiters MLG (c) and MLG–Wierse (d). As before, a qualitative improvement can be observed when using second order. Table II displays the comparison of the $L_1(\phi)$ errors of the numerical solutions on both grids. The same conclusions regarding accuracy as in the previous test can be drawn in this case.

4.3. Steady hydraulic jump with steady solute transport over flat and frictionless bed

This test case is used to check the behaviour of the solutions in the presence of a rapidly varying flow. A supercritical uniform flow, over flat and frictionless bed, is deflected by a solid wall at an angle σ generating an oblique hydraulic jump as shown in Figure 4.

There is an exact relationship between the water depths upstream the shock, h_1, and downstream of it, h_2, the Froude number of the incoming flow normal to the jump, Fr_1, and the angle formed by the jump, ς

$$\frac{h_2}{h_1} = \frac{1}{2}\left(\sqrt{1 + 8Fr_1^2 \sin^2 \varsigma} - 1\right) \tag{54}$$

and there is also an exact relationship between the deflection angle σ and the jump angle ς:

$$\tan \sigma = \tan \varsigma \frac{\sqrt{1 + 8Fr_1^2 \sin^2 \varsigma} - 3}{2\tan^2 \varsigma - 1 + \sqrt{1 + 8Fr_1^2 \sin^2 \varsigma}} \tag{55}$$

DOI: 10.1002/fld

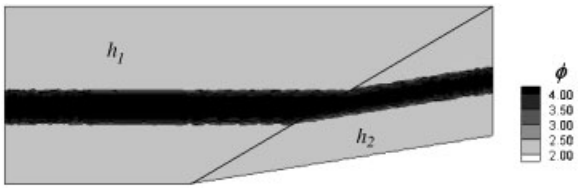

Figure 5. Exact solution for the solute concentration.

A continuous rate of solute inflow is assumed in a part of the inlet by means of an upstream boundary condition, defined by the function:

$$\phi\,(x=0,t)=\begin{cases}4, & 2\leqslant y\leqslant 3\\ 2, & y<2,\ y>3\end{cases} \tag{56}$$

The performance of the gradient slope limiters in the second-order methods is tested by means not only of the quality of the numerical water surface discontinuity but also by that of a discontinuity in the solute concentration that must follow the direction of the flow velocity and remain focused in the absence of diffusion.

The steady flow numerical solution is obtained in a first run from initial values of water depth h_1 and velocity v_1, after 10 s of simulation, enough to converge to the steady condition where the oblique hydraulic jump is developed. In this case, the upstream and downstream depths are, respectively $h_1=1$ and $h_2=1.5$ with $Fr_1=2.74$. The deflection angle is $\sigma=8.95^\circ$ and the jump angle is $\varsigma=30^\circ$.

In a second run, the solute injection is initiated and the solute is transported along the channel as a plume that follows the velocity deflection. No diffusion is assumed. Figure 5 shows the computational domain, 16 m long and 5.5 m wide, discretized in 14 474 triangular cells. It also displays the jump position and the exact solution.

Figure 6 displays 2D contour plots of the solute concentration using first order with CFL = 3 (a), second order using the MLG–Wierse limiter over the solute concentration alone (CFL = 1/3) (b), and second order using the MLG–Wierse limiter over the solute concentration alone (CFL = 1/3) (c). Second-order approach provides the most accurate results.

Table III shows the numerical L_1 error over the solute concentration in order to compare the efficiency of the different approaches. It can be seen that both the use of second order over the full set of conserved variables and only over the solute concentration provide more accurate results than first order as expected.

At the same time, Table III shows that second order only over the solute concentration provides the best results, although the interpolation over the set of conserved variables does not reduce strongly the accuracy of the solution. This is a good example of the influence between the conserved variables when using a coupled formulation.

On the other hand, Table IV compares the error in the water depth numerical solutions when, for second order of accuracy the interpolation is always performed over the set of conserved variables including or not the solute concentration.

The quality of the solution for the water depth is strongly reduced when enforcing second order over the conserved variables including the variable solute concentration as the correct definition of the mass solute interpolation planes reduces the solution to first-order approach in many cases.

DOI: 10.1002/fld

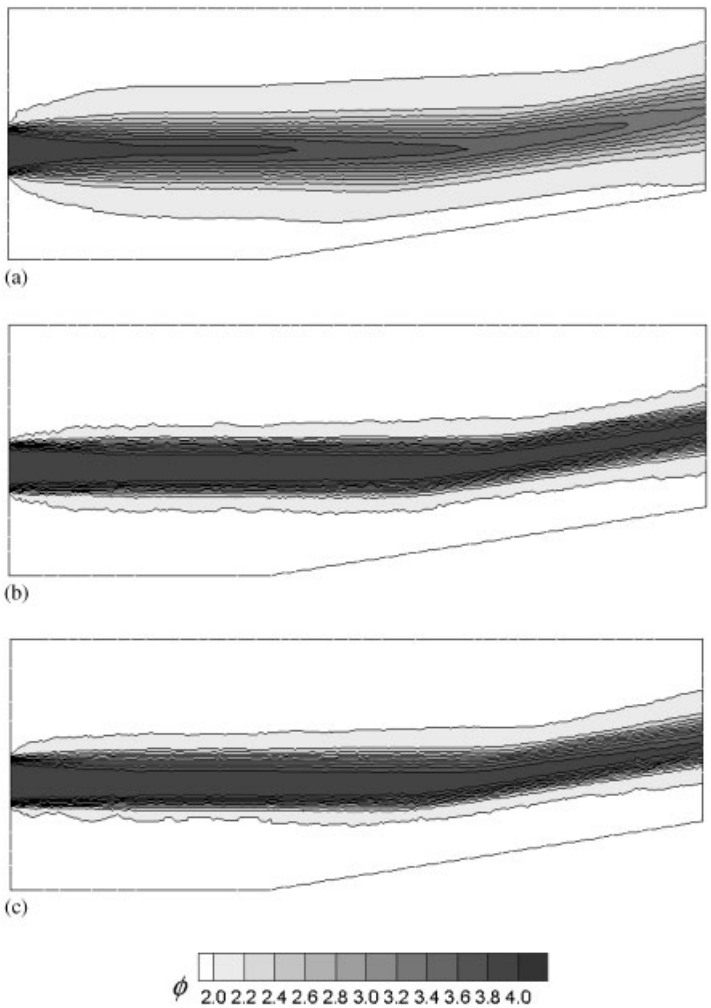

Figure 6. (a) 2D contour plots of ϕ using first order with CFL = 3; (b) second order over the solute concentration using the MLG–Wierse limiter (CFL = $\frac{1}{3}$); and (c) second order over all the variables using the MLG–Wierse limiter under the same conditions (CFL = $\frac{1}{3}$).

Table III. $L_1(\phi)$ function using first and second order over the set of conserved variables and over the solute concentration.

Interpolated variables/$L_1(\phi)$	First order (CFL = 1)	First order (CFL = 3)	MLG (CFL = $\frac{1}{3}$)	MLG–Wierse (CFL = $\frac{1}{3}$)
$h, hu, hv, h\phi$	14.945	14.944	7.735	8.212
ϕ	14.945	14.944	6.730	7.611

DOI: 10.1002/fld

Table IV. $L_1(h)$ function using first and second order over the set of conserved variables and over the solute concentration.

Interpolated variables/$L_1(h)$	First order (CFL = 1)	First order (CFL = 3)	MLG (CFL = $\frac{1}{3}$)	MLG–Wierse (CFL = $\frac{1}{3}$)
$h, hu, hv, h\phi$	0.895	0.898	0.677	0.721
h, hu, hv ($\phi = 0$)	0.895	0.898	0.364	0.491

The error in the solution for both water depth and solute concentration is the same when using values of CFL smaller or larger than one in first-order approach with independence of the presence of solute concentration, as expected.

4.4. Instantaneous injection of concentration in a channel with uniform flow

In this test case the influence of the order of approximation and the time step used is evaluated in the presence of a non-zero diffusion coefficient. The instantaneous injection of a mass M at time t_0 at a point (x_0, y_0) in an unbounded channel with uniform flow of velocity, $\mathbf{u}(x, y, t) = (u_0, 0)$, and water depth, $h(x, y) = h_0$, from a situation of clear water is simulated. The exact solute concentration variation in space and time is given by [1].

$$\phi_\infty(x, y, t) = \frac{M}{h_0 4\pi t\sqrt{K_x K_y}} \exp\left(-\frac{(y - y_0)^2}{4K_y t}\right) \exp\left(-\frac{(x - x_0 - u_0 t)^2}{4K_x t}\right) \tag{57}$$

where K_x and K_y are the coefficients of the diffusion matrix $\mathbf{K}$, defined as

$$\mathbf{K} = \begin{pmatrix} K_x & 0 \\ 0 & K_y \end{pmatrix} \tag{58}$$

The analytical solution for a channel of width B is [22]:

$$\phi(x, y, t) = \sum_{m=-\infty}^{\infty} \phi_\infty(x, y - mB, t) \tag{59}$$

A channel 4 m long and 1 m wide is used to compare the solutions from both first- and second-order schemes for the advective part combined with an implicit discretization of the diffusion terms. The coordinate origin is located at the left-bottom corner. The water depth in the entire channel is $h_0 = 1$ m and the water velocity is $u_0 = 1$ m/s. The mass injected is $M = 1$.

In the first numerical experiment the initial condition for the concentration is given by the exact solution (57) evaluated at $t = 3$ s using the hypothesis that the injection is located at $x_0 = -2$ m and $y_0 = 0.5$ m so that the initial ϕ distribution is centred at $x = 1$ m and $y = 0.5$ m. The simulation is carried on from that time up to $t = 5$ s. A constant diffusion coefficient is assumed, $K_x = 0.001\,\mathrm{m}^2/\mathrm{s}$, also $K_x = K_y$. As in this case the water depth and velocity are uniform and constant in the entire domain, no differences can be noticed if second order is imposed on the conserved variable $h\phi$. Figure 7 shows the exact solution for the solute concentration distribution at $t = 5$ s (a), the result using second order over solute concentration with the MLG–Wierse slope limiter (b), and using first order with CFL = 3 (c). In this case solute advection is strongly dominant. First order gives

DOI: 10.1002/fld

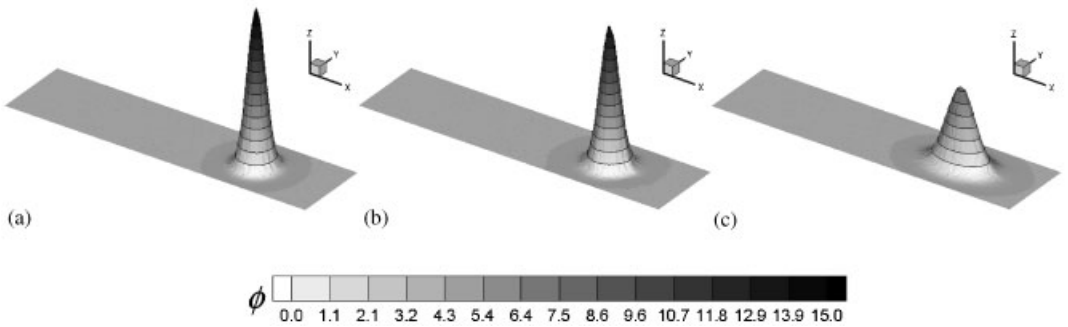

Figure 7. $K_x = 0.001$ m^2/s, $t = 5$ s: (a) exact solution; (b) numerical solution using second-order MLG–Wierse limiter with CFL $= \frac{1}{3}$; and (c) numerical solution using first order with CFL $= 3$.

Table V. L_1 error and maximum solute concentration for different values of K_x and numerical techniques.

	$K_x = 0.001$		$K_x = 0.01$		$K_x = 0.1$	
	L_1	$\phi^{\max}$	L_1	$\phi^{\max}$	L_1	$\phi^{\max}$
MLG, CFL $= \frac{1}{3}$	0.0676	14.2838	0.0186	1.9521	0.0701	0.5604
MLG–Wierse, CFL $= \frac{1}{3}$	0.1029	13.9068	0.0165	1.9557	0.0679	0.5625
First order, CFL $= 1$	0.5980	7.6234	0.1254	1.6782	0.0825	0.5534
First order, CFL $= 2$	0.5782	7.7987	0.1283	1.6729	0.0804	0.5547
First order, CFL $= 3$	0.5696	7.8751	0.1352	1.6600	0.0796	0.5552

a poor representation of the solution. Table V shows how the L_1 error is smaller and the solute concentration peak is higher when enforcing second order than when using first-order approach.

In the second numerical experiment, the initial condition is given by the exact solution with an injection point located at $x_0 = -1$ m and $y_0 = 0.5$ m, and evaluated at $t = 2$ s so that the initial ϕ distribution is centred at $x = 1$ m and $y = 0.5$ m. The simulation finishes at $t = 4$ s. The diffusion coefficients are constant, $K_x = K_y = 0.01$ m^2/s. Figure 8 shows the exact solution for the solute concentration at $t = 4$ s (a), the numerical result obtained using second order over solute concentration with the MLG–Wierse slope limiter (b), and using first order with CFL $= 3$ (c). In this case, first order preserves better the shape of the exact solution compared with the previous experiment. Table V shows how the L_1 error is smaller and the solute concentration peak is higher when enforcing second order than when using first-order approach.

In the third numerical experiment, the initial condition is given by the exact solution with an injection point located at $x_0 = 0$ m and $y_0 = 0.5$ m, and evaluated at $t = 1$ s so that the initial ϕ distribution is centred at $x = 0.5$ m and $y = 0.5$ m. The simulation ends up at $t = 3$ s. The diffusion coefficient in this case is extremely high $K_x = 0.1$ m^2/s and $K_x = K_y$. Figure 9 shows the exact solution for the solute concentration at $t = 3$ s (a), the numerical result obtained using second order over solute concentration with the MLG–Wierse slope limiter (b), and using first order with CFL $= 3$ (c). There is no visual difference when comparing first- and second-order solutions.

DOI: 10.1002/fld

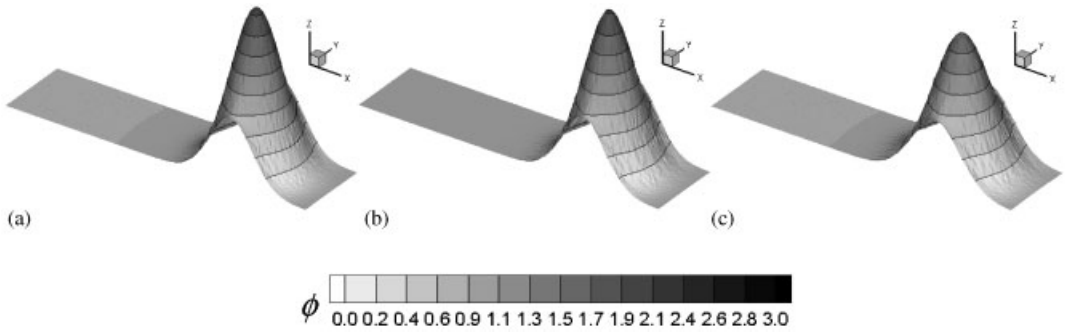

Figure 8. $K_x = 0.01$ m^2/s, $t = 4$ s: (a) exact solution; (b) numerical solution using second-order MLG–Wierse limiter with CFL $= \frac{1}{3}$; and (c) numerical solution using first order with CFL $= 3$.

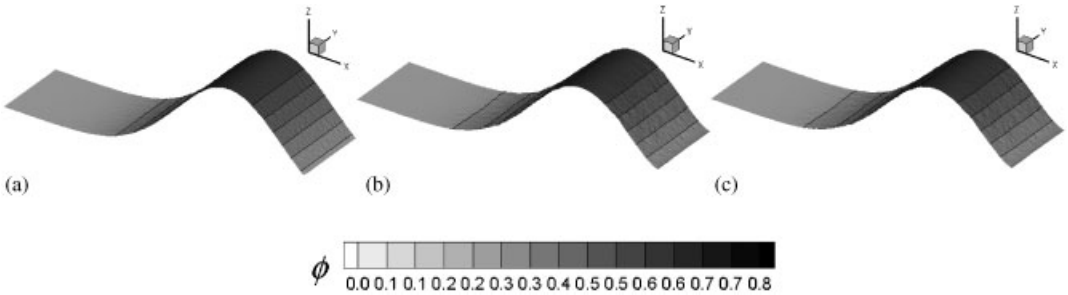

Figure 9. $K_x = 0.1$m^2/s, $t = 3$s: (a) exact solution; (b) numerical solution using second-order MLG–Wierse limiter with CFL $= \frac{1}{3}$; and (c) numerical solution using first order with CFL $= 3$.

Table V shows how the L_1 error is still smaller and the solute concentration peak is still higher when enforcing second order than when using first-order approach, but the differences between first and second order are not as high as in the other cases.

4.5. 1D frictionless dam break with non-uniform solute concentration over flat bed

The quality of the numerical solutions of the water flow and solute concentration variation in unsteady flow and in the presence of strong gradients of both water depth and solute mass for first- and second-order approximations is analysed involving a 1D dam break problem with exact solution. The discontinuous initial water depth and the initial solute concentration are defined by the following functions:

$$h(x) = \begin{cases} 5, & x < 0 \\ 50, & x \geqslant 0 \end{cases}, \quad \phi(r) = \begin{cases} 0, & x < 0 \\ 100, & x \geqslant 0 \end{cases} \tag{60}$$

where x is the distance from the centre of the domain. Figure 10 shows the exact distribution for both water depth and solute concentration at the initial time (left) and after 40 s considering no

DOI: 10.1002/fld

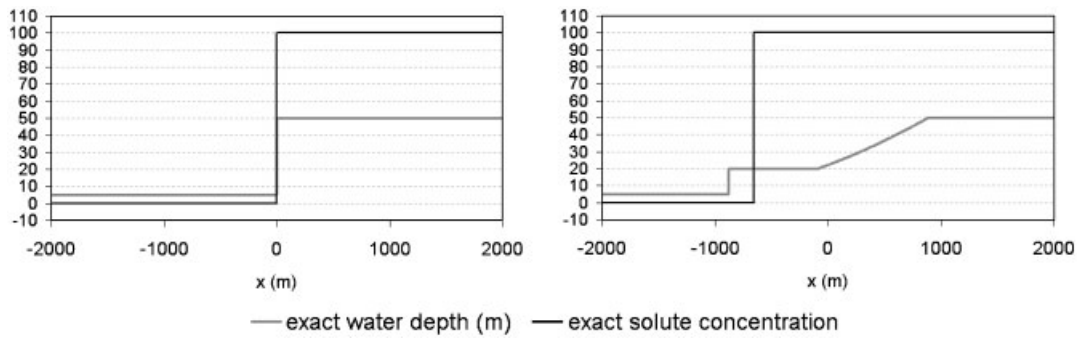

Figure 10. Initial water depth and solute concentration (left) and exact water depth and solute concentration after 40 s (right).

solute diffusion (right). Not considering that the solute evolution has an influence over the flow dynamics, the solution corresponds to the ideal dam break wave [23] for water depth and water velocity plus a discontinuous solute front advancing more slowly than the water front [24].

The numerical solutions have been computed in a squared domain $4000 \times 4000\ \mathrm{m}^2$ using a triangular unstructured mesh divided into 32 672 cells. When using first-order approach no meaningful differences appear in the solution either for small or large values of CFL as Figure 11(a) shows. Figure 11(b) and (c) shows the solution obtained by enforcing second order over the solute concentration and over the set of conserved variables. No visual differences in the solution are observed. Second order provides more accurate solutions than first order does, although the accuracy gain is not as effective as in the steady cases.

4.6. Long wave resonance in a circular parabolic frictionless basin with solute

The analytical solution of a long wave resonating in a circular, frictionless parabolic basin was presented by Thacker [25] for the shallow water equations, where the free surface displacement is given by

$$\zeta(r,t) = \zeta_0 \left(\frac{(1-A^2)^{1/2}}{1 - A\cos\omega t} - 1 - \frac{r^2}{a^2} \left\{ \frac{1-A^2}{(1-A\cos\omega t)^2} - 1 \right\} \right) \tag{61}$$

and the basin shape is given as

$$z(r,t) = -\zeta_0 \left(1 - \frac{r^2}{a^2} \right) \tag{62}$$

with $A = (a^4 - r_0^4)(a^4 + r_0^4)^{-1}$ and $\omega = a^{-1}\sqrt{8g\zeta_0}$, where ζ_0 is the centre point water depth, r is the distance from the centre point, a is the radial distance from the centre point to the zero elevation on the shoreline and r_0 is the distance from the centre point to the point where the water depth is initially nil. Those values are represented in Figure 12(a). The numerical values used for this test are $\zeta_0 = 20.0$ m, $r_0 = 1200$ m, $a = 1500$ m. The domain is divided into triangular cells of $l = 25$ m generated using the discretization shown in Figure 12(b).

DOI: 10.1002/fld

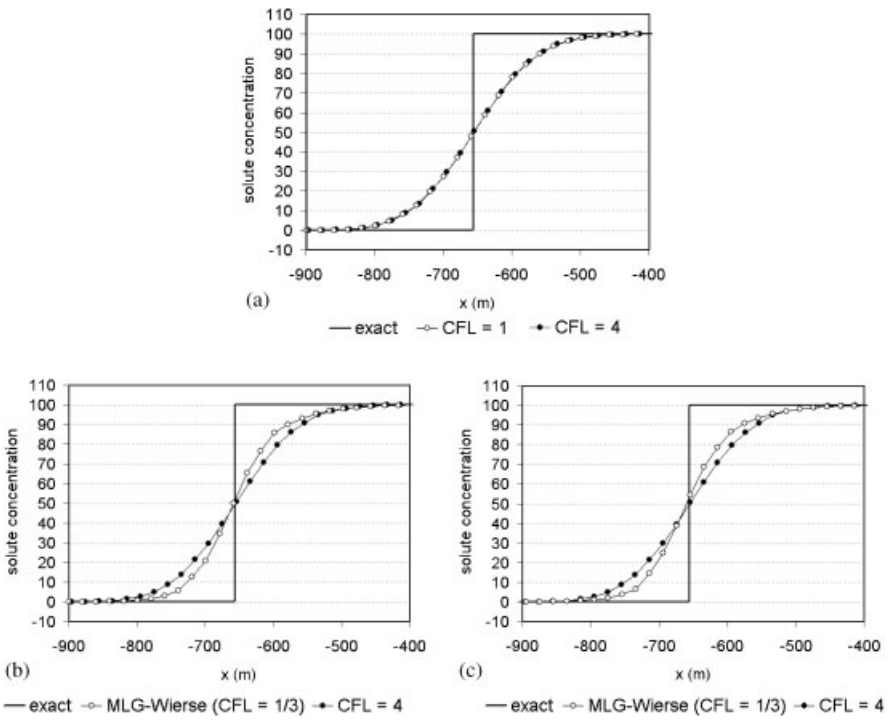

Figure 11. (a) Solute concentration profile using first order approach; (b) using second order over the solute concentration; and (c) using second order approach over the set of conserved variables after 40 s.

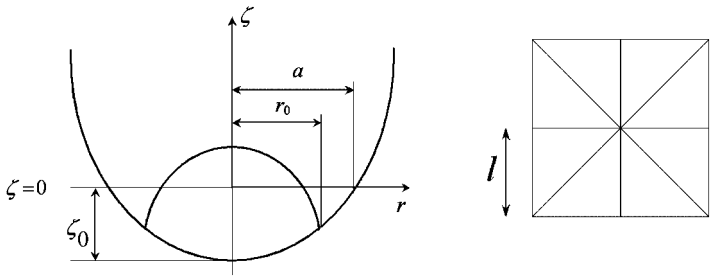

Figure 12. Sketch of the initial free surface and water depth profile for the parabolic basin test (left) and detail of the mesh discretization (right).

At the same time, an initial solute concentration is assumed, given by

$$\phi(r) = \begin{cases} 2, & r < 600 \\ 1, & r \geqslant 600 \end{cases} \tag{63}$$

that is also the exact solution after each period, as no diffusion is considered. Figure 13(a) shows a 3D view of the exact solute concentration, the numerical solute concentration computed with fully first order (b), the solution for fully second order, that is, over the set of conserved variables (c)

DOI: 10.1002/fld

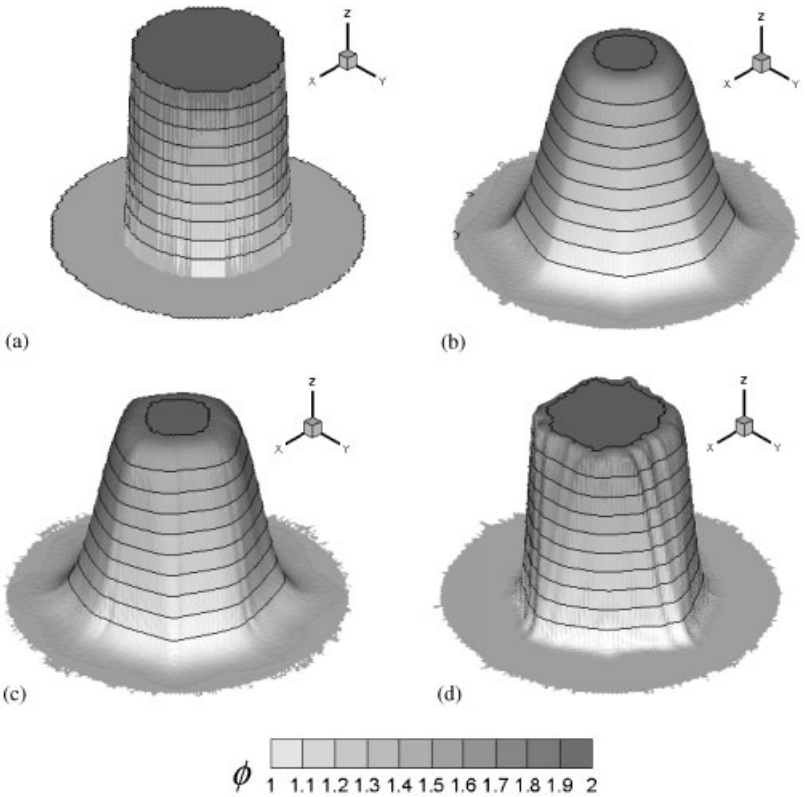

Figure 13. (a) 3D view of the exact solute concentration; (b) solution for the solute concentration using first order; (c) solution for the solute concentration using second order over all the variables; and (d) solution for the solute concentration using second order over the solute concentration after 4T.

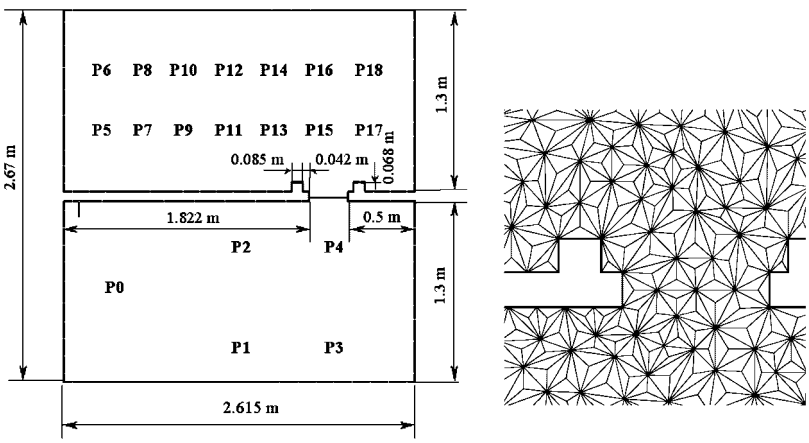

Figure 14. Model geometry (left) and detail of the mesh (right).

DOI: 10.1002/fld

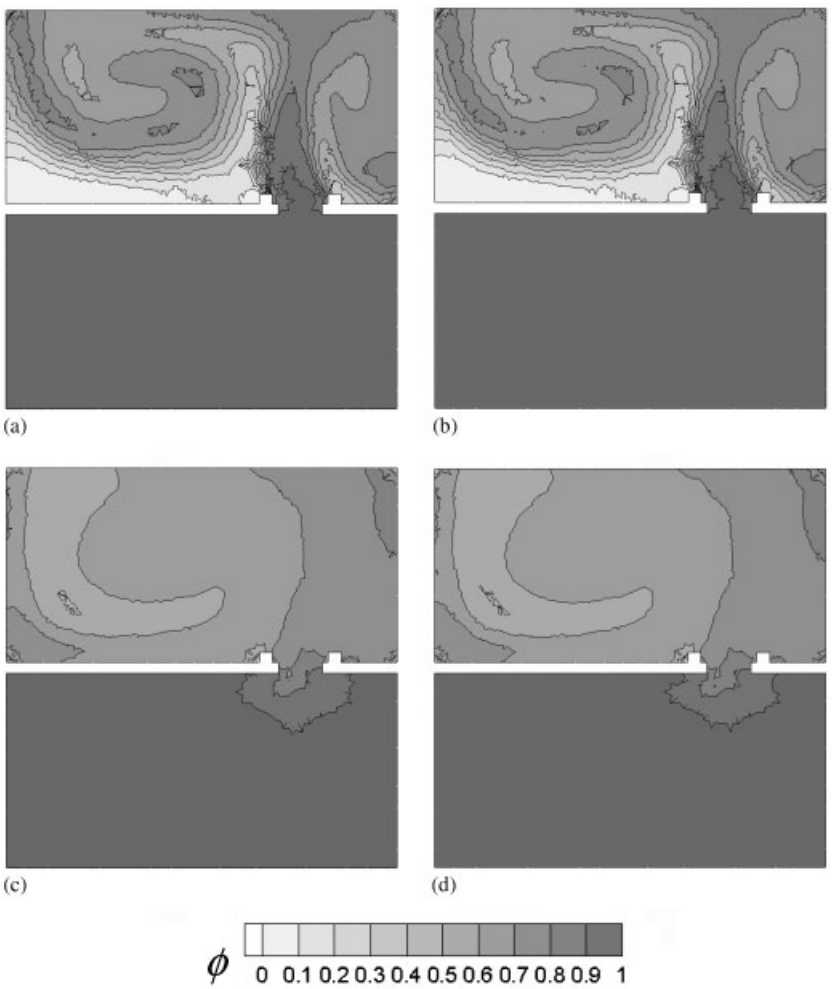

Figure 15. (a) Solute concentration computed using first order (CFL = 4) at $t = 5$ s and (c) at $t = 12$ s and (b) using second-order MLG–Wierse over the solute (CFL = $\frac{1}{3}$) at $t = 5$ s and (d) at $t = 12$ s.

and the solution using a second-order representation only over the solute concentration (d) after 4T. Almost no differences appear between the results obtained using first and second order over the set of conserved variables. The number of limitations required to satisfy a correct construction of the interpolating planes lead to a severe reduction of the second-order approach. On the other hand, if second order is only enforced over the solute concentration a marked increment in the accuracy of the solution is observed.

4.7. Asymmetric dam break in a laboratory model

The following test case for the proposed model deals with the transport of solute by a 2D dam break flow problem. The dam break flow experiment was carried out at the CITEEC, Coruña,

DOI: 10.1002/fld

Spain [26]. The set-up consists of a flat bed closed pool divided into two parts (Figure 14 left) by a removable gate. The experiment was performed for an initial depth ratio of 0.5/0.1 m assuming a Manning roughness parameter $n = 0.01$. A distribution of solute, not present in the experiment, has been assumed in this example, where an initial solute ratio of 2.0/1.0 is defined. In this example, flow is unsteady and both the water level and solute are initially discontinuous. On the other hand, the flow domain is permanently confined within vertical walls so that the solution is free from any wet/dry boundary effect.

The mesh consists on 7875 cells. A detail of the spatial discretization can be seen in Figure 14 (right). Figure 15(a) and (c) shows the solutions obtained using first order with approach CFL = 4, at time $t = 5$ and 12 s after the gate removal, respectively, while Figure 15(b) and (d) shows the solutions using second-order approach over the solute concentration 5 and 12 s after the gate removal, respectively. The complexity of the flow in this case does not allow any remarkable improvement of the solution when using second-order approach.

5. CONCLUSIONS

A general formulation of finite volume schemes on triangular grids has been presented in order to study the relative performance of a first-order scheme and a MUSCL–Hancock scheme, theoretically of second order in space and time accuracy, as applied to unsteady and steady 2D shallow water flows with solute advection and diffusion in several situations.

As far as the non-diffusive part of the system is concerned, spatial second-order accuracy has been built using MLG and MLG–Wierse limited cell gradient methods (MUSCL). First order has been used both in the basic version and in the version extended to values of CFL>1. The diffusion terms have been discretized using an implicit centred technique.

Only one test case has been used to analyse the behaviour of the numerical solutions in the presence of physical diffusion. The results confirm that, in the simple conditions of steady uniform flow a second-order approach produces an improvement in the accuracy of the numerical solution less noticeable for extremely high diffusion coefficient values.

A brief analysis of the form in which the source terms get involved in the time step restrictions has been included and extended to the coupled system of shallow flow/solute transport. At the same time an efficient way to avoid unbounded values of solute concentration within the framework of the second-order scheme has been presented.

Two test cases of non-uniform steady shallow water flow with smooth water surface and pure advective transport of an initially sinusoidal solute cloud have been used to demonstrate the superiority of the second-order technique in the resolution of the solute distribution evolution. The results are rather similar when using the two options of applying second order over the full set of conserved variables or only over the solute concentration variable.

In cases of transient shallow water flow over complex geometry and wet/dry fronts the fully second-order method over all the variables is not the best option to accurately track the solute evolution. Instead, a first-order representation for all the variables except the solute distribution is recommended in these cases. The test case of long wave resonance in a parabolic basin has been useful to see this effect. At the same time, the proposed conservative redistribution strategies have proved valid and useful to be able to calculate at the standard time step rate.

In the same line, when both the water level and solute distribution are discontinuous in steady state, our study indicates that numerical results more accurate than first order in all the variables

DOI: 10.1002/fld

cannot be achieved simultaneously. However, a noticeable gain in the quality of the solute results is obtained by using a second-order representation only in this variable.

In cases of discontinuous unsteady flow, the application of a second-order method does not bring any improvement in the numerical results. A first-order method provides satisfactory results and is very competitive when used in the version extended to CFL>1.

ACKNOWLEDGEMENTS

This work was partially funded by the INCLAM company and by the Spanish Ministry of Science and Education through the Research Project CGL2005-07059-C02-02.

REFERENCES

1. Rutherford JC. *River Mixing*. Wiley: New York, 1994.
2. Murillo J, Burguete J, Brufau P, García-Navarro P. Coupling between shallow water and solute flow equations: analysis and management of source terms in 2D. *International Journal for Numerical Methods in Fluids* 2005; **49**:267–299.
3. Néelz S, Wallis SG. Taking accuracy of a semi-Lagrangian method for advection–dispersion modelling in rivers. *International Journal for Numerical Methods in Fluids* 2006; **53**(1):1–21.
4. Nair RD, Scroggs JS, Semazzi FHM. A forward-trajectory global semi-Lagrangian transport scheme. *Journal of Computational Physics* 2003; **190**(1):275–294.
5. Oliveira A, Fortunato AB. Toward an oscillation-free, mass conservative, Eulerian–Lagrangian transport model. *Journal of Computational Physics* 2002; **183**:142–164.
6. Begnudelli L, Sanders F. Unstructured grid finite-volume algorithm for shallow-water flow and scalar transport with wetting and drying. *Journal of Hydraulic Engineering* 2006; **132**(4):371–384.
7. Courant R, Isaacson E, Rees M. On the solution of nonlinear hyperbolic differential equations by finite differences. *Communications on Pure and Applied Mathematics* 1952; **5**:243–255.
8. Murillo J, García-Navarro P, Brufau P, Burguete J. Extension of an explicit finite volume method to large time steps (CFL>1): application to shallow water flows. *International Journal for Numerical Methods in Fluids* 2005; **50**:63–102.
9. Murillo J, García-Navarro P, Burguete J, Brufau P. A conservative 2d model of inundation flow with solute transport over dry bed. *International Journal for Numerical Methods in Fluids* 2006; **52**(10):1059–1092.
10. Murillo J, García-Navarro P, Burguete J. The influence of source terms on stability, accuracy and conservation in 2d shallow flow simulation using triangular finite volumes. *International Journal for Numerical Methods in Fluids* 2007; **54**(5):543–590.
11. Benqué JP, Hauguel A, Violet PL. *Engineering Applications of Computational Hydraulics*, vol. II. Pitman: London, 1982.
12. Vreugdenhil CB. *Numerical Methods for Shallow-Water Flow*. Kluwer Academic Publishers: Dordrecht, 1994.
13. Brufau P, Vázquez-Cendón ME, García-Navarro P. A numerical model for the flooding and drying of irregular domains. *International Journal for Numerical Methods in Fluids* 2002; **39**:247–275.
14. Cunge JA, Holly FM, Verwey A. *Practical Aspects of Computational River Hydraulics*. Pitman: London, 1980.
15. Roe PL. Approximate Riemann solvers, parameter vectors and difference schemes. *Journal of Computational Physics* 1981; **43**(2):357–372.
16. García-Navarro P, Vázquez-Cendón ME. On numerical treatment of the source terms in the shallow water equations. *Computers and Fluids* 2000; **29**:951–979.
17. Hubbard ME, García-Navarro P. Flux difference splitting and the balancing of source terms and flux gradients. *Journal of Computational Physics* 2000; **165**:89–125.
18. Van Leer B. On the relation between the upwind-differencing schemes of Godunov, Enguist–Osher and Roe. *SIAM Journal on Scientific and Statistical Computing* 1985; **5**(1):1–20.
19. Batten P, Lambert C, Causon DM. Positively conservative high-resolution convection schemes for unstructured elements. *International Journal for Numerical Methods in Engineering* 1996; **39**:1821–1838.
20. Wierse M. A new theoretically motivated higher order upwind scheme on unstructured grids of simplices. *Advances in Computational Mathematics* 1997; **7**:303–335.

DOI: 10.1002/fld

21. Leveque RJ. *Numerical Methods for Conservation Laws*. Birkhäuser: Basel, 1990.
22. Fischer HB, Imberger J, List EJ, Koh RCY, Brooks NH. *Mixing in Inland and Coastal Waters*. Academic Press: Orlando, U.S.A., 1979.
23. Stoker JJ. *Water Waves*. Interscience: New York, 1957.
24. Toro EF. *Shock-Capturing Methods for Free-Surface Shallow Flows*. Wiley: New York, 2001.
25. Thacker WC. Some exact solutions to the non linear shallow water equations. *Journal of Fluid Mechanics* 1981; **107**:499–508.
26. Méndez PL, Brufau P, Puertas J. An experimental approach to the dam break problem. Real data to check numerical models. *XXIX IAHR Congress*, Beijing, China, 2001.

DOI: 10.1002/fld